Journal of Theoretical and Applied Vibration and Acoustics 1(2) 107-121 (2015)

I S A V

Journal of Theoretical and Applied Vibration and Acoustics

journal homepage: http://tava.isav.ir

Plume outflow intrusion impact on acoustical signal fluctuations in a pre-stratified environment

Mohmmad Akbarinasab *

Assistant Professor, Faculty of Marine & Oceanic Science, University of Mazandaran, Babolsar, Iran

KEYWORDS

Pre-Stratified

Environment

Outflow intrusions

Sound propagation

Trace envelope

Signal fluctuations

ABSTRACT

Existence of outflow intrusion introduces small-scale turbulence that perturbs the vertically stratified character of the sound velocity and causes spatial and temporal fluctuations of the sound propagation. In this experimental study, we have investigated acoustic wave propagation with frequency of 50 *kHz* in a pre-stratified environment with intrusion of a turbulent plume while the signals received in different locations and times are recorded. At first, a fourth-order Butterworth band-pass filter was applied to the received voltage time series. Then the signals received at different times when entering the outflow intrusion at similar depths are compared to the ones without plume intrusion. In order to investigate the shapes of the signals received at different moments of the experiment they are analyzed in the time domain using trace envelope techniques. The results show that if the transmitter is positioned in the outflow intrusion location, the received signals in the upper and lower part of the outflow intrusion show a signal amplitude increase but the received signals in the dyed outflow show a signal amplitude decrease. Thereby, results indicate that the outflow intrusion could be important in shapes of the received signals. Also we have observed the occurrence of major signals fluctuations over time is accordance with the sound speed vertical structure changes due to the intrusion development.

1. Introduction

Characterizing the acoustic signal propagation through water is essential for many applications including underwater acoustic communications, active and passive sonar, underwater navigation and tracking and ocean acoustic tomography. The highly time-varying nature of the underwater environment can cause many undesirable distortions to the propagating signal. Time-varying multipath distortions may be the result of dense reflections from rough surfaces, fluctuations in sound speed due to inhomogeneous media, relative motion between transmitters and receivers or changes in the propagating media [1]. Signal fluctuations could be caused by a number of physical processes including: source or receiver motion, oceanic fine-scale features, sea-surface

* Corresponding Author: M. Akbarinasab, Email: m.akbarinasab@umz.ac.ir

motion (waves and tides), scattering, internal waves and internal tides and ocean currents and eddies [2]. The ocean environment which includes water column, surface and bottom boundaries plays a vital role for operation of sonar. In fact the ocean environment models form as basis for sonar performance models, and the acoustic propagation models serve as a link between them. Unlike sea bottom characteristics which are considered time-invariant for sonar applications, the water column properties like temperature, salinity, density and currents are highly variable both in time and space [3]. Thermohaline intrusions are often observed in vertical profiles of temperature and salinity in the ocean. They are made visible by large fluctuations or inversions in the profiles and as zig-zag patterns in temperature–salinity plots. These features typically have vertical scales of 10–100 *m* and horizontal scales of 1–100 *km* [4]. In the presence of horizontal gradients of temperature and salinity, the intrusive signature may be produced by vertically-alternating lateral currents across ocean fronts. These interleaving motions are thought to be driven by buoyancy forces arising from perturbations in the density field, e.g. produced by differential mixing of heat and salt by double diffusion [5]. There have been few studies related to high frequency acoustic scattering from either salt fingers or through laminar and turbulent thermal plumes [6-9] but there are not any studies about the effect of a plume outflow on sound propagation in a pre-stratified environment. Today there are acoustic models which could be used to predict the sound propagation changes but all of them have problems because each of them uses approximation to calculate the acoustic intensity. In addition, the field experiments are too much expensive, thus using the laboratory experiments may help and are more economical. By some scaling the acoustic results of laboratory signals could be used for the real environment. (For example, a common method for evaluating scattering involves the factor $k_{lab}a_{lab} \approx k_{sea}a_{sea}$: k is the wave number and a is an effective radius of the scatter). There is no laboratory measurement about the sound propagation in the outflow intrusion in a pre-stratified environment. In this article, the effect of outflow intrusion from a plume in a pre-stratified environment on the sound propagation is investigated.

2. Laboratory set-up and methods

2.1. Laboratory set-up

All experiments were carried out in a glass tank 2.19 *m* long, 1.27 *m* wide and 0.8 *m* deep (Fig. 3). Before the experiments, six transducers (of which three of them are transmitters and the rest of them as receivers) are mounted opposite to each other with a separation of 1.65 *m* on two Iron bars inside the tank. The distance between the transducers is 0.14 *m*. These holders are facing each other at a distance 0.3 *m* from the tank wall. Prior to the beginning of the experiments with stratification, the acoustic measurements were executed in fresh water. All received signals were sampled at 5 *MHz* for all experiments. A fourth-order Butterworth band-pass filter was applied to the received voltage time series with cutoff frequencies at 45 and 55 *kHz* for the 50-*kHz* data. In case where a “filling box" stratification [10] is used, the tank was initially filled with fresh water to a depth of 0.48 *m*. The water was then stratified using a plume of dense salt solution falling from the end of the small tube (a nozzle of 3 *mm* diameter) placed at 0.47 *m* from the base with a buoyancy flux of F=g’*Vo= 5×10^{-7} m^4/s^3 . After setting up the “filling box" stratification in the tank (Fig. 1) acoustic signals and hydrophysical data were measured simultaneously. Then to produce the outflow intrusions, a source of dyed salt solution with a density less than the

previous case ("filling box") with volume flux of $2.1\times10^{-7}\ m^4/s^3$ was entered into the stratified environment. At the start of the experiment with plume intrusion, the speed of the nose of the outflow increased with time. The intrusion is also thickened and eventually split to generate a new tongue of dyed plume water growing beneath the first layer. The dye tracer in the outflow water was slowly adverted upward to replace water entrained into the plume at shallower depths and eventually reached to the source level. The outflow intrusion is produced at the start of the experiment at the location of the transmitter in the middle of the tank (at the depth of 0.22 *m*). The dyed outflow water is wedged-shaped with a sloping interface beneath. In different time intervals the acoustic and hydrophysics data are measured simultaneously and then these signals in different time based on the place of the plume outflow are processed.

2.2. Physical properties of the water tank

A device RS232 conductivity meters model 8301 was used for measurements of conductivity, temperature and pressure. Density (ρ) and sound speed (c) were also derived from these measurements by the formula of [11] and [12]. The salinity changes are the only factors that caused the received acoustic signals variations. Figure 1 shows the procedure of salinity and sound speed profile changes that were measured at different times at 70 *cm* distance from the entrance of the plume while the effects of intrusion were taken within the filling box stratification [10].

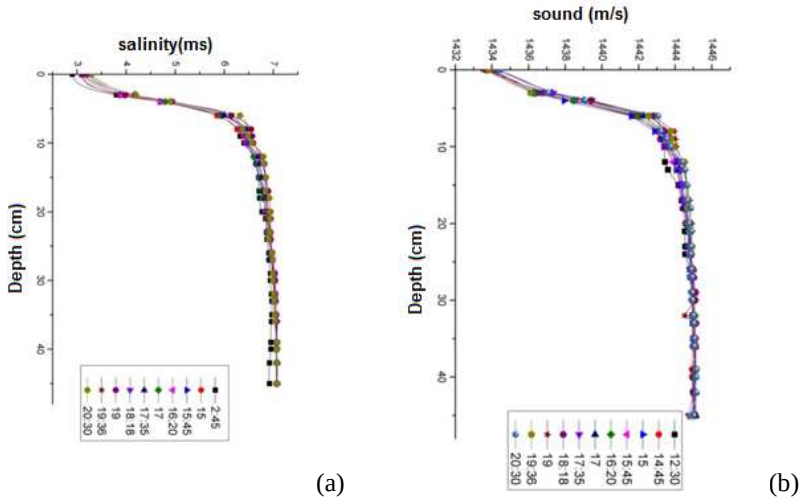

Fig.1. (a) The vertical profile of salinity and (b) The vertical profile of sound speed while the experiments are carried out with the filling box profiles (numbers are in hours:minutes from the start of experiment)

As Figure 1 shows, the profiles of salinity and sound speed in the water tank are the same. The coefficient of correlation between salinity and sound speed is 0.99 which shows the sound speed variation in the tank is controlled by salinity changes.

2.3. The non-dimensional parameters of the intrusive flow

The non-dimensional parameters governing the outflow intrusion in an enclosure c are the Prandtl number $pr = \frac{\upsilon}{k_T}$ (υ is the kinematic viscosity and k_T is the diffusivity of component T), the aspect ratios $\frac{H}{L}$ and $\frac{H}{W}$ (L and W are the length and width of the tank respectively and H is the flow depth), the dimensionless plume buoyancy flux $F_p = \frac{F'}{H^4 N_0^3}$ with the buoyancy flux as $F' = Og' = Q(\Delta\rho/\rho)g$, Q as the volume flux of the plume source and N_0 as the buoyancy frequency of the environment calculated from the "filling box" solution by the following formula [13]:

$$N = F^{1/3} \times (2E)^{(-2/3)} \pi^{(-1/3)} D^{(-4/3)} [2.18(z/D)^{(-5/3)} + 0.279(z/D)^{(-2/3)} + 0.083(z/D)^{(1/3)} .....]^{(1/2)} \quad (1)$$

F is the plume buoyancy flux and z the vertical direction. In addition, the measure of the scattered ultra convection to molecule is calculated by the Peclet number: $Pe = F'^{1/3} H^{2/3}$ similar with the Reynolds number. The outflow velocity is calculated by the following equation [13]:

$$U = 1.37 \times E^{1/3} \times F^{1/3} H^{1/6} W^{1/2} \quad (2)$$

F is the plume buoyancy flux, E is the entrainment coefficient, H is the height of fall of the plume and W is the width of the tank. The plume entrainment coefficient is also about 0.1. For the "filling-box" gradient, the stratifying plume source was placed at H = 0.47 m above the bottom of the tank and the supplied buoyancy flux was:

$$F = Qg' = Q\,\Delta\rho/\rho\, g = 2.1 \times 10^{-7} \times 20/1000 \times 10 = 4.4 \times 10^{-8}\, m^4/s^3 \quad (3)$$

The initial profile of the buoyancy frequency is $N_0(z = H) = 6.6 \times 10^{-5} s^{-1}$. The dimensionless plume buoyancy flux for the outflow intrusion is $F_p = \frac{F'}{H^4 N_0^3} = 0.0342$. In this experiment, the depth of the plume was 0.47 m and the buoyancy flux was $4.4 \times 10^{-8}\, m^4/s^3$ and the width of the tank is 127 cm and the outflow velocity could be calculated as:

$$U = 1.37 \times E^{1/3} \times F^{1/3} H^{1/6} W^{1/2} = 1.37 \times 0.1^{1/3} \times (4.4 \times 10^{-8})^{(1/3)} 0.46^{1/6} 1.27^{1/2} = 0.0022\, m/s \quad (4)$$

2.4. The setup of the acoustic systems

The relatively small dimensions of the water tank provide some problems with the acoustic reflections. Not only the surface and the bottom reflect the acoustic signals, but the side wall reflections have to be taken into consideration because of the proximity of the tank walls. The

wall reflections can interfere with the surface reflections, therefore, we use non-directional transducers with consideration of the layers which are established by the outflow intrusion and is in a scale order of centimeters. Hence the acoustic signal must be sampled by higher frequency in order to study the effect of the intrusion in the stratified region on the sound propagation in such a confined region. The radius of non-directional transducers used in the experiment was 3.5 *cm* with 50 *kHz* center frequency (Type 50B5NR, Furuno). Since these sensors are sensitive to angel of propagation and in addition to prevent the layers mixture, the two holders are mounted separately on two iron bars outside the outflow intrusion and the transmitters are before the plume outflow and receivers are installed in front of the transmitter at the end of the tank (Fig. 2). The schematic of this set up is shown in Fig. 2.

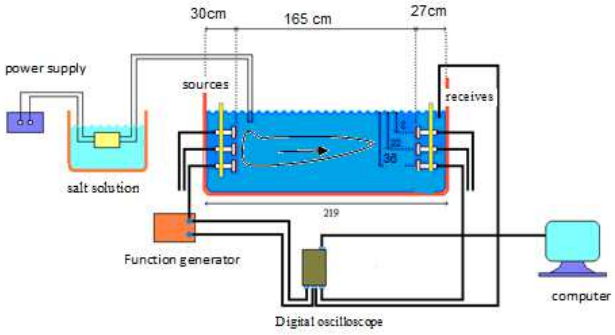

Fig. 2. A sketch of the experimental set-up

Table 1. Transducer and general experimental parameters.

Frequency(kHz) Center	200	50
Spatial resolution(cm)	0.7	3
Transducer diameter, D (cm)	3.5	3.5
Far field, D^2/λ	17.5	4
First Fresnel radius, $\sqrt{\lambda r_{scat}}$	9.16	18.97
Full beamwith, θ	6.6	13
Pulse length (μs)	50	**190**
wave	Burst of sine wave	**Burst of sine wave**
Number of packet	10	**10**
Peak to peak signal	20	**20**

In this experimental study, acoustic signals were recorded at frequencies 50 *KHz* and 200 *KHz* in a pre-stratification environment before introducing the turbulent plume. Different scenarios were tested to measure the acoustic signals that are as follows:

a: Source depth is 8 *cm* and receiver depths are 8, 22 and 36 *cm*.

b: Source depth is 22 *cm* and receiver depths are 8, 22 and 36 *cm*.

c: Source depth is 36 *cm* and receiver depths are 8cm, 22 and 36 *cm*.

2.5. Investigation of model 50B5NR transducers directivity

Directivity helps us to determine the bearing of the target and reduces the noise in desired directions. Different formulations are presented based on the piezoelectric transducers with different designs and variation of their directivity. In this experiment, a circle of traducers with radius of 3.5 *cm* is used and the similar directivity of this kind of transducers in the horizontal and vertical directions, due to homogeneity of the surface of the transmitted wave, is calculated as follows [14],

$$B(\theta) = \left[\frac{2J_1(ka \sin\theta)}{ka \sin\theta} \right]^2 \tag{5}$$

where J_1 is the Bessel function of the first kind and k is the wave number of the working frequency which is equal to $k = \frac{2\pi f}{c}$. By using this formulation, the transducer directivity at frequencies 50 *kHz* and by attention to its radius of 3.5 *cm*, the beam pattern of the output is calculated and its shape is shown in Fig. 3.

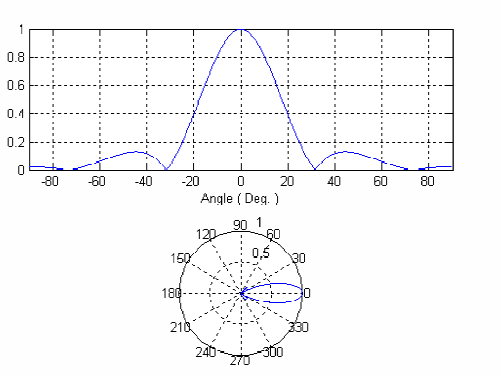

Fig. 3. Beam pattern of the transducer with 50 kHz center frequency

The transducer directivity at 50 *kHz* is 26 degree based on Fig. 3. (In +13◦.,-13◦ related to acoustic axis, the intensity is reduced by 3db). By using this angel, the part of the tank depth which is under the effect of acoustic emission could be calculated. In this experiment, the distance between receiver and transmitter is 1.65 *m*, thereby $x = \arctan(13) \times 1.65 = 0.38m$ .In this case, for this frequency, 0.38 *m* of water thickness horizontally and vertically are under the beam of the acoustic source.

2.6. The characteristics of the generated signal

The source transducer was powered by a Function 20 *MHz*/Arbitrary Waveform Generator Model DG 1022 set to generate 10 cycles of sinusoid bursts at frequency of 200 *kHz* and 50 *kHz* with amplitude of 20 volts peak-to-peak where the pulse duration was chosen according to the geometric constraints of the tank and the sampling rate was 5 *MHz*. The pulse is repeated with duration of 100 *ms* allowing enough time between received pulses for the tank reverberations to diminish. The received signals and those feeding the transmitter were continuously recorded in digital forms. Such recording allowed us to measure the absolute travel time of propagation

using signal processing. Higher frequencies are favored because of greater resolution in the time of arrival separations between the direct signals and reflected one from other surfaces with the smaller acoustic wavelengths.

2.6.1. Investigation of the water tank principal reflections and travel times

As it was said in the introduction, the first step of experiment was with no plume that enters the environment; the acoustic signal was gathered in the homogeneous (fresh) water environment. Since there is no salt in the environment which cause the signal path changes, the first signal received is related to direct signal path .The further signals which were observed on the display of oscilloscope were because of reflection and scattering from bottom, surface and the walls as it is seen in Fig. 4 [15] [15].

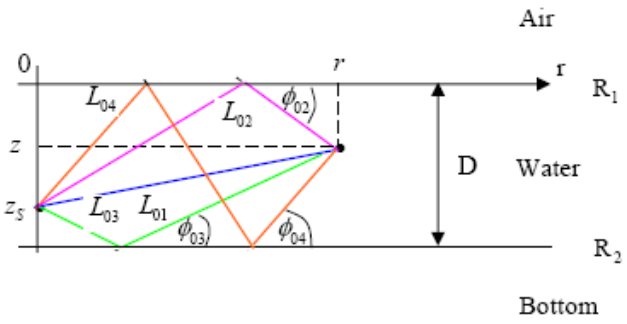

Fig. 4. The geometry of the principal tank reflections.

Figure 4 shows a schematic representation of the contributions from the physical source at depth z_s and the four paths which come from this source indirectly at the receiver with depth of z and at a horizontal distance of r from the source. The first path is the direct path (L_{01}). The second path is via the surface that is reflected and then reaches to the reviver (L_{02}). The third path is through the first hit from the bottom and after reflection reaches the receiver (L_{04}). The fourth path hits the surface and then the bottom, and finally it is received at the receiver. The lengths of these paths are calculated as follows.

$$L_{01}=\sqrt{r^2+(z_s-z)^2},\quad L_{02}=\sqrt{r^2+(z_s+z)^2},\quad L_{03}=\sqrt{r^2+(2D-z_s-z)^2},$$
$$L_{04}=\sqrt{r^2+(2D+z_s-z)^2} \tag{6}$$

As the path is assumed to be *m*:

$$L_{m1}=\sqrt{r^2+(2Dm-z_s+z)^2},\quad L_{m2}=\sqrt{r^2+(2Dm+z_s+z)^2},\quad L_{m3}=\sqrt{r^2+(2D(m+1)-z_s}$$
$$L_{m4}=\sqrt{r^2+(2D(m+1)+z_s-z)^2} \tag{7}$$

D in these relations is the depth of the channel.

The travel time of each ray path is the duration in which that ray reaches the receiver that can be easily calculated. From the above discussion it is revealed that the signal of direct path arrives

earlier than other paths. Travel times for all the rays can be easily computed by knowing the lengths of the rays and the velocity of each ray. Thereby, we can write expressions for the travel times as follows:

$$T_{m1} = L_{m1}/C, \quad T_{m2} = L_{m2}/C, \quad T_{m3} = L_{m3}/C, \quad T_{m4} = L_{m4}/C \tag{8}$$

3. Results of measurements of acoustic signals

In order to compare different acoustic signals at different times and locations with different conditions, first the transmitted signal is measured in homogeneous water. Then, based on the receivers' and transmitters' distances from each other and the above formulation, the travel time of each ray path is analyzed and investigated. Fig. 5 shows a typical example of the input and the output signal from a source at a depth of 0.8 *m* and a receiver at the depth of 0.8 *m*.

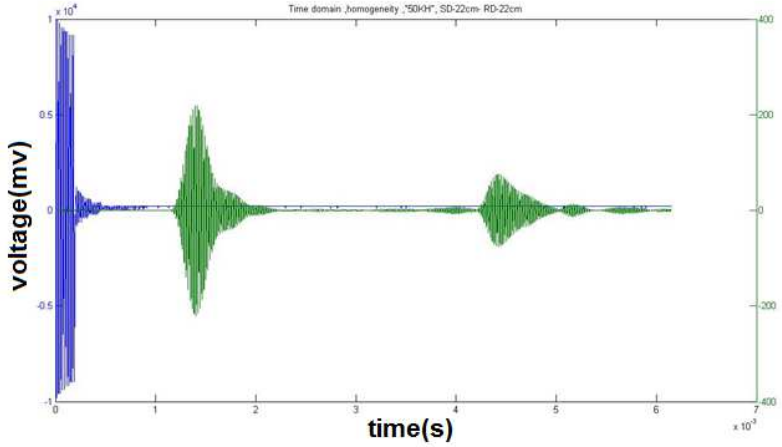

Fig. 5. The recorded signal at frequency 50kHz in fersh water. The blue represent the transmitter at the depth 0.8 m and the green represent the recieved signal at the depth 0.8 m.

Figure 6 shows the distances between transmitters and receivers in the acoustic signal measurement scenarios.

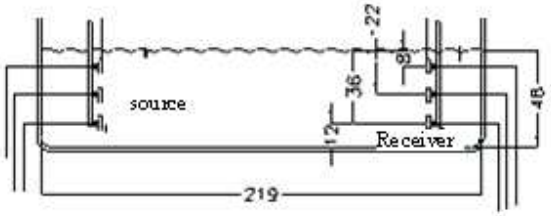

Fig. 6. The distance between transmitters and recivers in the acoustic signal

Note that the distance between transmitter and receiver is 1.65 *m* and assuming a sound speed of 1375 *m/s* given the water tank typical water temperature of approximately 22° C, thus:

$$t_1 = \frac{x_0}{c} = 1.65 \diagup 1375 = 1.2ms \tag{9}$$

The delay time t_1 is distance between start of input signal and start of the first received signal (Fig. 6).Thereby the first envelope in Fig. 7 represents the direct transmitted pulse. The second envelope in Fig. 6 is the wave reaching the receiver after reflection from the back wall of the receiver and thus, since the hydrophones do not have any receiving backward path (because the receivers are non- directional) the ray hits the wall in front of the transmitter and by the repeated reflection it reaches the front of hydrophone as is observed in the output. The total distance traveled is thus $x = 1.65 + 0.27 + 0.27 + 1.65 + 0.3 + 0.3 + 1.62 = 6.6$. Hence $t_1 = x/c = 6.6/1375 = 4.8ms$.

As it is shown in Fig. 6, these time delays are precisely on the start time of the second envelope, thus, this conclusion is yielded that in order to investigate the inhomogenity of the environment on the reflections, the variations of the first envelope must be investigated. In order to find out where each of these envelopes are backscattered using the ray theory which is presented in section 2.6.1 and by programming the time delay of each received signal in receiver it is calculated after the passing wave. The results of this calculation are shown in Table 2.

Table 2. The distances and travel times of main reflections of the acoustic signals by the walls of the water tank.

Reflection	Direct			Surface			Bottom			Surface-Bottom		
Receiver(cm)	8	22	36	8	22	36	8	22	36	8	22	36
Distance (m))(at the source of depth-8cm)	1.65	1.65	1.67	1.65	1.65	1.67	1.83	1.77	1.73	1.9	1.78	1.78
Distance (m))(at the source of depth - 22cm)	1.65	1.65	1.65	1.7	1.7	1.74	1.73	1.73	1.69	1.9	1.9	1.84
Distance (m))(at the source of depth - 36cm)	1.65	1.65	1.65	1.7	1.74	1.8	1.73	1.69	1.66	2.06	1.93	1.9
Travel Time (ms)(at the source of depth - 8cm)	1.2	1.2	1.2	1.2	1.2	1.24	1.3	1.29	1.25	1.38	1.29	1.29
Travel Time (ms)(at the source of depth - 22cm)	1.2	1.2	1.2	1.2	1.24	1.27	1.25	1.25	1.25	1.9	1.38	1.34
Travel Time (ms)(at the source of depth - 36cm)	1.2	1.2	1.2	1.2	1.2	1.3	1.3	1.2	1.2	1.5	1.4	1.4

3.1. The influence of the outflow intrusion on sound signals

When the signals received at different locations and times are recorded, first a fourth-order Butterworth band-pass filter was applied to the received voltage time series with cutoff frequency of 45 and 55 *kHz* for 50-*kHz* BB data. The effects of inhomogeniety are investigated by comparing the signals received in different times when entering the outflow intrusion at similar depths. Two samples of these signals are analyzed as in the following. The other ones are given in Table 2. In these figures, all signals are normalized to their maximum magnitudes. Fig. 7 shows at the left panel, typical shapes of the signals received at different times of the experiment, while the transmitter is located at depth of 0.08 *m* (at the upper part of the dyed outflow position) and the receiver is located at depth of 0.22 *m* (and it is on the opposite side the dyed outflow). At the right panel, photographs of the evolution of a salt outflow into a "filling box" salt gradient are shown at different times of the experiment. The plume source water was marked with red dye. Under these circumstances, the amplitude envelope of the first signal is reduced and the wave front time of the signal is shifted to right due to the sound speed increase at the location of the dyed outflow (0.22 *m*). The sound ray is bended towards the direction of the sound speed reduction and thus peak to peak of the signal is reduced instant by instant as it enters the plume (increasing the sound speed). Since at this depth, the internal waves are also generated, the time of the wave front is recorded at 1.5 *ms*.

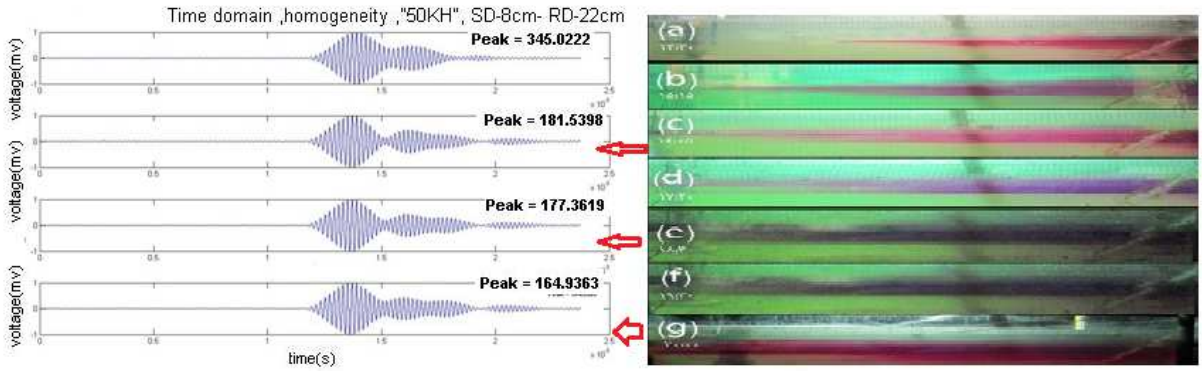

Fig. 7. Left panel, shapes of the signals received at different times of the experiment and the right panel shows evolution of a salt outflow into a "filling box" salt gradient at different times (source is at depth of 0.08 *m* and reciver is at depth of 0.22 *m*). The amplitudes shown are normalized by the mximum amplitude of the corresponding signals. The outflow intrusion images were taken at time :16.20 simultanious with right figure at frame (C);18.30 simultanious with left frame (e), and (d); 20.30 simultanious with right frame on frame (g).

In order to investigate the shapes of the signals received at different times of the experiment, they have been analyzed in time domain by using the trace envelope techniques. A trace envelope is a mathematical estimate of a bounding curve for the signal and is computed using the Hilbert transform that computes the complex analytical trace [16] and [17], and then takes the absolute value. Figure 8 shows the trace envelopes for fresh water and different times of the outflow intrusion. Note that by passing the ray through the outflow intrusion, the third envelope is shifted to the right and at time 1.5 *ms* the amplitude of signal is increased momentarily. Also, in order to show the signals variation better, we have shown in Fig. 9, the spectrogram of the output signal based on Fig. 8 in the frequency domain, indicating the reduction of the signals due to the outflow.

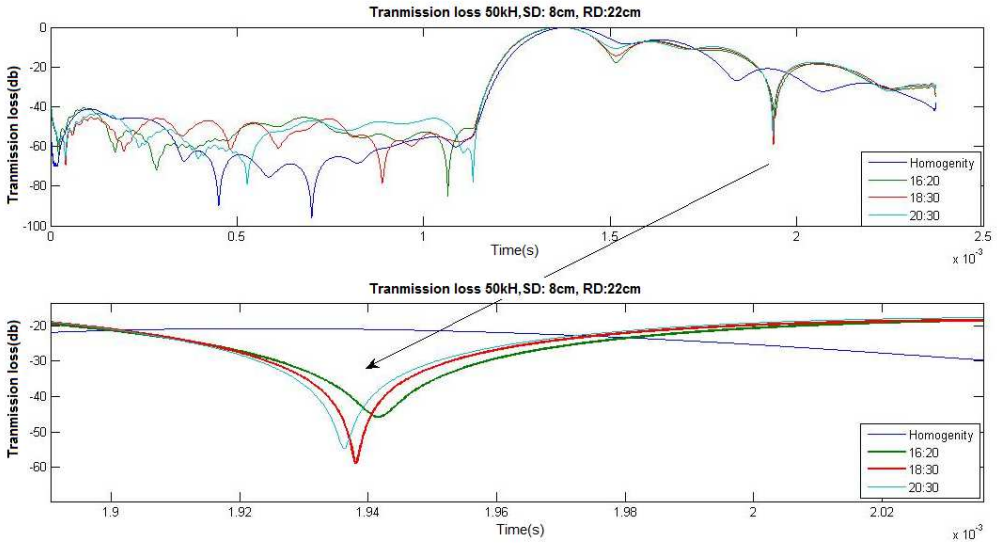

Fig. 8. The envelopes of the four traces of Fig. 8 plotted on a decibel scale. From top to bottom, for homogeneous water; and the case with intrusion at times: 16.30 (green curve); 18.30 (red curve); 20.30 (green curve)

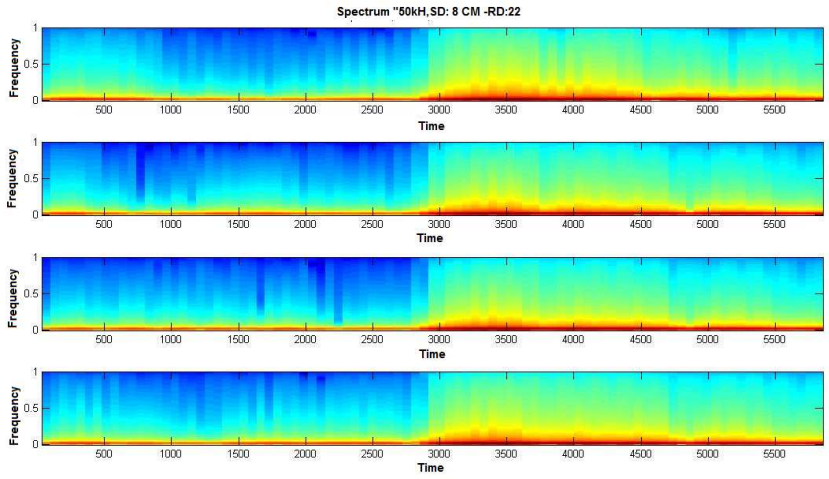

Fig. 9. Spectrogram of received acoustic signal (transmitter at depth of 0.08 *m* and receiver at depth of 0.22 *m*) from top to bottom at homogeneous water and at times: 16.30, 18.30, 20.30 from the start of intrusion

Figure 10 shows typical shapes of the signals received at different times of the experiment and the evolution of a salt outflow into a "filling box" salt gradient at different moments of the experiment when the transmitter is located at depth of 0.22 *m* and the receiver is located at depth of 0.36 *m*. On the right panel, the outflow intrusion images during experiment are shown. All the observed differences in the propagation time and energy level of the signals are mainly caused by the changes in the position of outflow intrusion. We see that the received signal consists of two distinct wave packets, one centered at t=1.4 *ms* which is the first mode, and the other centered at t=1.7 *ms*, which is the second mode. There is also a weak third-mode with arrival

centered at t=2.2 *ms*. Note that the travel-time estimated from the dispersion curves are consistent with the computed time series. Note also that the peak amplitude of the second wave packet is higher at the first moment as compared to the other signals but with time this amplitude was decreased and as the peak amplitude of the first wave packet was added, the length of output pulse was reduced instantly. Figure 11 shows the spectrogram of received acoustic signals when the transmitter is at depth of 0.22 *m* and receiver is at depth of 0.36 *m*.

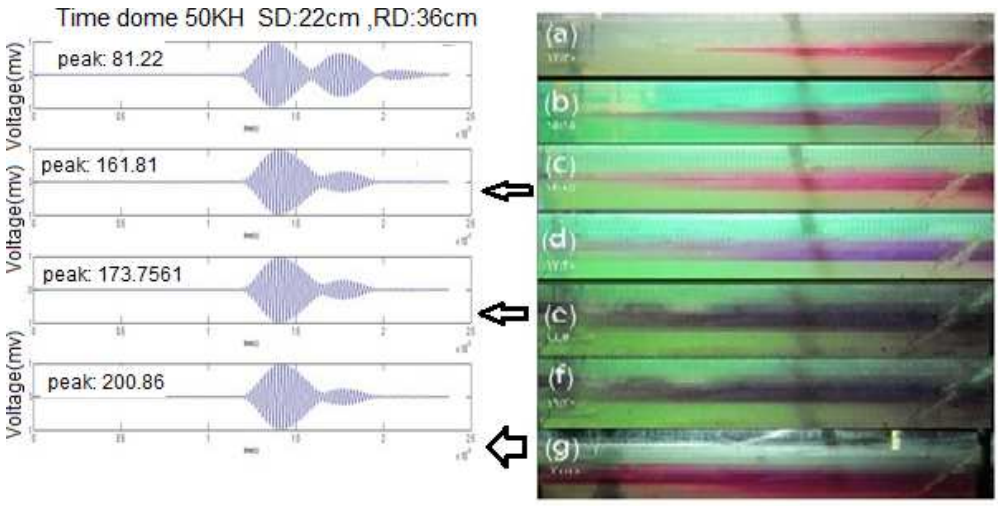

Fig. 10. Left panel, shapes of the signals received at different moments of the experiment and right panel, the evolution of a salt outflow into a "filling box" salt gradient atdifferent moments of the experiment (source is at depth of 0.22 *m* and reciver is at depth of 0.36 *m*).The amplitudes shown are normalized.

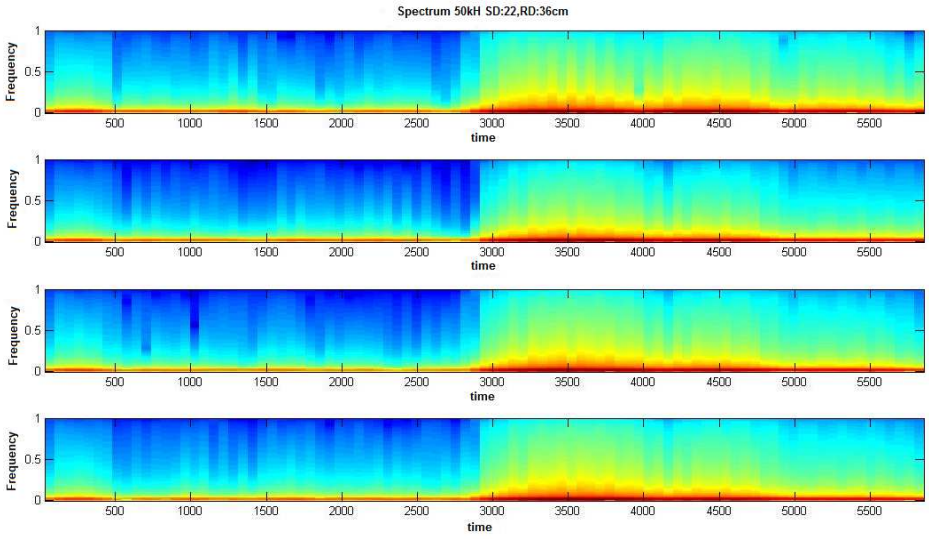

Fig. 11. Spectrogram of received acoustic signal (transmitter at depth of 0.22 *m* and receiver at depth of 0.36 *m*) from top to bottom at homogeneous water and at times: 16.30-18.30-20.30 from the start of the intrusion

Table 3 shows peak to peak variations of signal in homogeneous water and also in case of the filling box for different moments of plume intrusion.

Table 3. The peak to peak variations of signal for the whole experimental set-ups

Transmitter depth (cm)-receiver depth(cm)	peak to peak of output signal at homogeneous water(mv)	peak to peak of output signal at time the filling box (mv)	peak to peak of output signal at time 16:20 (mv)	peak to peak of output signal at time 18:30 (mv)	peak to peak of output signal at time 20:30 (mv)
8-8	495.67	333.74	416.22	404.84	378.66
8-22	344	140.75	183.11	179.06	166.39
8-36	277.36	142.75	185.24	180.04	165.4
22-8	324.2	460.78	368.76	380.07	399.37
22-22	440	304.61	366.33	352.77	324.94
22-36	80.33	233.75	163.06	174.29	201.24
36-8	155.82	312.26	225.16	251.43	275.45
36-22	315	193.01	226.36	222.09	209.07
36-36	152.67	135.3	126.27	126.36	123.92

Based on Table 3 and Fig. 7, it is revealed that when the transmitter is located at 0.08 *m* and the receiver is located at every depth, as time passes, the amplitude of the received signal is reduced because, at the receiver location the sound speed is lower and the rays are bended towards the lower speed direction, thus the rays have no tended to move to the receivers side. In this case, it is observed that when the transmitter is at the depth of 0.08 *m* and the receiver at the depth of 0.08 *m*, the amplitude of signal is reduced by 35 mv compared to the initial samples, but when it is located at other depths, the amplitude of signal is reduced less. When the transmitter is located at the depth of 0.22 *m* (the place of the increased sound velocity and possibly internal wave generation) and the receiver is at depth of 0.08 *m* , the amplitude of signal at the receiver is increased, since at the receiving point the sound speed is lower than at the transmitting point, thus higher rays reached the receiver, but in the case when the receiver is at the depth of 0.22 *m* , the amplitude of signal at the receiver is decreased since at the receiving point there is no tendency to move to this direction because of increased sound velocity. When the receiver is at depth of 0.36 *m* (below of the dyed outflow) the amplitude of signal is increased. In third scenario, the transmitter is located at depth of 0.36 *m* in this case when the transmitter is at 0.08 *cm* the amplitude of signal is increased instantly, in this case at the receiver location the sound

speed is lower than that of transmitting location thus as a result the rays are bended up more and more, but when the receiver is located at 0.22m, the waves amplitude is decreased, because this wave front cause the rays bended towards the bottom. Also the received signal is reduced , in this scenario if we change the position of the receiver to the depth of 0.36 m, the amplitude of signal in an instant that the dyed outflow does not intrude to this depth is increased but when the dyed outflow intrude to this depth the amplitude of signal is decreased.

4. Conclusion

In this study, our aim was to analyze the signals received at frequency 50 *KHz* by a linear array over time in order to detect variations in the information content of such signals and, if possible, to find out correspondence between these fluctuations and the changes of outflow intrusion features. In general, it was found that the occurrence of outflow intrusion altered the propagation characteristics of acoustic waves and different position of transmitter and receiver leads to very different results.

The main findings of these experiments are:

1-When the transmitters are located at different depths, but the receiver located at the front of the outflow intrusion at the same depth, the amplitude of received signal as the time passes is decreased, but if transmitter is located in dyed plume and the receivers at the upper and lower of the intrusion front of outflow, the amplitude of output signal with the plume outflow development is increased with time (Snell's law).

2- We have also observed the occurrence of major signals fluctuations over time in accordance with the sound speed vertical structure changes during the outflow development.

3-The outflow from semi-enclosed seas as the Persian Gulf outflow with thickness of about 45 meters [18] and its seasonal variations may also change the acoustic paths in such regions and the results of these experiments may be used to clarify such changes. Although one should be careful as these experiments are carried out in a confined region, while actual outflow happens in the open sea. The results of this simulation could be used with consideration of the acoustic scale rule $k_{lab}a_{lab} \approx k_{sae}a_{sea}$.

References

[1] L.M. Brekhovskikh, I.P. Lysanov, Fundamentals of ocean acoustics, Springer Science & Business Media, 2003.
[2] P.C. Etter, Underwater acoustic modeling and simulation, CRC Press, 2013.
[3] C.V.K. Prasada Rao, Modelling of coastal ocean environment for underwater surveillance, Indian Journal of Marine Sciences, 39 (2010) 616.
[4] K.N. Fedorov, The thermohaline finestructure of the ocean: Pergamon marine series, Elsevier, 2013.
[5] B.R. Ruddick, J.S. Turner, The vertical length scale of double-diffusive intrusions, Deep Sea Research Part A. Oceanographic Research Papers, 26 (1979) 903-913.
[6] A.C. Lavery, T. Ross, Acoustic scattering from double-diffusive microstructure, The Journal of the Acoustical Society of America, 122 (2007) 1449-1462.

[7] T. Ross, R. Lueck, Sound scattering from oceanic turbulence, Geophysical Research Letters, 30 (2003).
[8] H.E. Seim, M.C. Gregg, R.T. Miyamoto, Acoustic backscatter from turbulent microstructure, Journal of Atmospheric and Oceanic Technology, 12 (1995) 367-380.
[9] J.D. Warren, T.K. Stanton, P.H. Wiebe, H.E. Seim, Inference of biological and physical parameters in an internal wave using multiple-frequency, acoustic-scattering data, ICES Journal of Marine Science: Journal du Conseil, 60 (2003) 1033-1046.
[10] W.D. Baines, J.S. Turner, Turbulent buoyant convection from a source in a confined region, Journal of Fluid Mechanics, 37 (1969) 51-80.
[11] C.T. Chen, F.J. Millero, Speed of sound in seawater at high pressures, The Journal of the Acoustical Society of America, 62 (1977) 1129-1135.
[12] N.P. Fofonoff, R.C. Millard, Algorithms for computation of fundamental properties of seawater, (1983).
[13] A.B.D. Wong, R.W. Griffiths, G.O. Hughes, Shear layers driven by turbulent plumes, Journal of Fluid Mechanics, 434 (2001) 209-241.
[14] C.S. Clay, H. Medwin, Acoustical oceanography: principles and applications, John Wiley & Sons, 1977.
[15] P.K. Pullarao, Modeling and simulation of an underwater acoustic communication channel, in: Department of Electrical Engineering and Computer Science, University of Applied Sciences, Bremen, Germany, 2004.
[16] M.T. Taner, F. Koehler, R.E. Sheriff, Complex seismic trace analysis, Geophysics, 44 (1979) 1041-1063.
[17] L. Cohen, Time-frequency analysis, Prentice hall, 1995.
[18] A.S. Bower, H.D. Hunt, J.F. Price, Character and dynamics of the Red Sea and Persian Gulf outflows, Journal of Geophysical Research, 105 (2000) 6387-6414.